



Minerva Access is the Institutional Repository of The University of Melbourne

**Author/s:**

Mann, SK;Czuba, E;Selby, LI;Such, GK;Johnston, APR

**Title:**

Quantifying Nanoparticle Internalization Using a High Throughput Internalization Assay

**Date:**

2016-10-01

**Citation:**

Mann, S. K., Czuba, E., Selby, L. I., Such, G. K. & Johnston, A. P. R. (2016). Quantifying Nanoparticle Internalization Using a High Throughput Internalization Assay. *Pharmaceutical Research*, 33 (10), pp.2421-2432. <https://doi.org/10.1007/s11095-016-1984-3>.

**Persistent Link:**

<https://hdl.handle.net/11343/282777>

**Quantifying Nanoparticle Internalization using a High Throughput  
Internalization Assay**

Sarah K. Mann<sup>1,2,3</sup>, Ewa Czuba<sup>1,3</sup>, Laura I. Selby<sup>1,3</sup>, Georgina K. Such\*<sup>2</sup> and Angus P.

R. Johnston\*<sup>1,3</sup>

<sup>1</sup>Drug Delivery, Disposition and Dynamics, Monash Institute of Pharmaceutical  
Sciences, Monash University, Parkville, Victoria 3052, Australia. E-mail:

angus.johnston@monash.edu

<sup>2</sup>Department of Chemistry, The University of Melbourne, Parkville, Victoria 3010,  
Australia. E-mail: gsuch@unimelb.edu.au

<sup>3</sup>ARC Centre of Excellence in Convergent Bio-Nano Science and Technology,  
Monash University, Parkville, Australia

## **ABSTRACT**

**Purpose** The internalization of nanoparticles into cells is critical for effective nanoparticle mediated drug delivery. To investigate the kinetics and mechanism of internalization of nanoparticles into cells we have developed a DNA molecular sensor, termed the Specific Hybridization Internalization Probe - SHIP.

**Methods** Self-assembling polymeric 'pHlexi' nanoparticles were functionalized with a Fluorescent Internalization Probe (FIP) and the interactions with two different cell lines (3T3 and CEM cells) were studied. The kinetics of internalization were quantified and chemical inhibitors that inhibited energy dependent endocytosis (sodium azide), dynamin dependent endocytosis (Dyngo-4a) and micropinocytosis (5-(N-ethyl-N-isopropyl) amiloride (EIPA)) were used to study the mechanism of internalization.

**Results** Nanoparticle internalization kinetics were significantly faster in 3T3 cells than CEM cells. ~90% of the nanoparticles associated with 3T3 cells were internalized, compared to only 20% of the nanoparticles associated with CEM cells. Nanoparticle uptake was via a dynamin-dependent pathway, and the nanoparticles were trafficked to lysosomal compartments once internalized.

**Conclusion** SHIP is able to distinguish between nanoparticles that are associated on the outer cell membrane from nanoparticles that are internalized. This study demonstrates the assay can be used to probe the kinetics of nanoparticle internalization and the mechanisms by which the nanoparticles are taken up by cells. This information is fundamental for engineering more effective nanoparticle delivery

systems. The SHIP assay is a simple and a high-throughput technique that could have wide application in therapeutic delivery research.

**KEY WORDS** nanoparticles – internalization – endocytosis – sensor – inhibitor

## **ABBREVIATIONS**

DBCO	Dibenzocyclooctyl
FIP	Fluorescent Internalization Probe
MFI	Mean Fluorescence Intensity
NaN <sub>3</sub>	Sodium azide
NP	Nanoparticle
PDEAEMA	Poly(2-(diethylamino) ethyl methacrylate)
PEGMA	Poly(poly(ethylene glycol) methacrylate)
PFPMMA	Pentafluorophenyl methacrylate
QP <sub>C</sub>	Complementary Quencher Probe
QP <sub>M</sub>	Mismatched Quencher Probe
RAFT	Reversible Addition-Fragmentation chain Transfer
Tf	Transferrin
SHIP	Specific Hybridization Internalization Probe

## **INTRODUCTION**

The use of nanoparticles (NPs) in medicine, particularly in drug-delivery, has potential to significantly enhance current treatment options and thus is a growing area of research interest(1, 2). Encapsulating a drug inside a NP has a number of

advantages over the conventional delivery of naked therapeutics : 1) the NP can protect the drug from degradation by the body; 2) targeted delivery of the NP to the site of action can limit potentially harmful side effects ; and 3) controlled release of the drug from the NP can maintain the optimal therapeutic levels of drug for extended periods of time. Whilst traditional small-molecule drugs enter cells primarily via passive diffusion through the cell membrane or by active transport through membrane protein channels, most nanoparticles enter cells via the energy dependent pathway of endocytosis(3). In this process the NPs are enveloped by the lipid bilayer of the cell membrane and internalized into an endosomal compartment. In order to design smarter materials for drug delivery it is essential to have a fundamental understanding of the kinetics of endocytosis and the mechanisms used by the cells to internalize the NPs.

A major challenge for studying the internalization of NPs is distinguishing between NPs that are simply associated with the cell surface, as opposed to NPs that have been taken up inside the cell. High resolution microscopy combined with cell surface staining can be used to investigate NP internalization, however this process is time consuming, and it can be challenging to determine if NPs are close to the cell membrane because they are in the early stages of endocytosis or if they are simply localized on the surface of the cell. High throughput techniques such as flow cytometry can analyze thousands of cells a second, however it only measures the total fluorescence intensity of the cell and does not directly give localization information. To overcome this limitation, a number of flow cytometry protocols have been adapted to study internalization using flow cytometry(4, 5), however they are either limited to studying a single fluorophore, eliminating the possibility of phenotyping, or are only

applicable to certain materials or cell types. To address these limitations we recently developed a method to track internalization of particles using a nucleic acid sensor, termed the specific hybridization internalization probe (SHIP) assay(6). In this assay particles are functionalized with the fluorescent internalization probe (FIP), a single stranded 20 base-pair oligonucleotide containing a 5' Cyanine 5 dye. After incubation of NPs with cells, a complementary quenching probe (QP<sub>C</sub>) is added to specifically quench the fluorescence of the FIP on the cell surface. The fluorescence intensity of the cells with and without QP<sub>C</sub> are then measured using flow cytometry, and the ratio of quenched to non-quenched fluorescence can be used to determine the percent of internalization. Using the SHIP assay, we have previously demonstrated the ability to distinguish cell membrane associated NPs from internalized NPs and compared the SHIP assay to traditional methods for determining internalization(6). SHIP has been adapted to study antibody-dependent phagocytosis(7), and we have also used SHIP to study the internalization of proteins and to relate the immune response of a model vaccine to the levels of endocytosis of different surface receptors on dendritic cells(8). As outlined above, a key challenge of nanomedicine research is understanding internalization pathways. It is still not fully understood whether manipulating such pathways could lead to more effective delivery systems. The SHIP assay provides a simple and high throughput tool to perform fundamental investigation into internalization processes. In this study, we have demonstrated the potential of the SHIP assay to study the internalization kinetics of NPs into different cell types, and investigate the mechanism by which the NPs are internalized into the cells using different internalization inhibitors.

We have focused our study on modular, pH-responsive ‘pHlexi’ nanoparticles, however the SHIP technique would be amenable to a range of polymer or inorganic nanoparticles. pHlexi particles are composed of two polymeric components: a pH responsive poly(2-diethylamino)ethyl methacrylate (PDEAEMA) polymer and a - poly(poly(ethylene glycol) methacrylate)-b-PDEAEMA (PEGMA-b-PDEAEMA) copolymer. pHlexi particles have been investigated for biomedical applications as they are synthesized using a modular, one-pot nanoprecipitation method that readily allows incorporation of therapeutics, they demonstrate tunable pH disassembly under physiological conditions and display endosomal escape capabilities(9).

Cells can use multiple endocytic pathways to take up NPs, and the endocytosis pathway has been shown to depend on the physicochemical characteristics of nanoparticles such as size(3), shape(10, 11) and charge(12). The four main endocytic pathways that have been implicated in NP internalization are macropinocytosis, clathrin-dependent endocytosis, caveolae-dependent endocytosis, and clathrin- and caveolae-independent endocytosis(13). Understanding which of these pathways are involved in NP uptake is critical to engineering smarter delivery systems that can respond to biological stimuli and deliver their therapeutic cargo when and where it is required. A common method to study endocytosis is to use chemical inhibitors that block specific steps in the endocytosis pathway(14). To demonstrate the utility of SHIP to study endocytosis pathways, we have chosen to three different inhibitors, sodium azide ( $\text{NaN}_3$ ), which inhibits all energy dependent internalization pathways, Dyngo-4a, which inhibits dynamin dependent pathways (such as clathrin and caveolin), and 5-(N-ethyl-N-isopropyl)amiloride (EIPA), which inhibits macropinocytosis. As the efficiency and mechanism of NP internalization also

depends on cell type, we studied the behavior of NPs in two cell lines; 3T3 (mouse fibroblast), and CEM (human T-lymphoblast). We compared nanoparticle behavior with two controls (calcein and transferrin (Tf)) that are known to be processed through macropinocytosis and clathrin dependent endocytosis respectively.

The SHIP assay allowed investigation of the internalization kinetics of pHlexi NPs which was found to differ significantly between the two cell types. Furthermore, the SHIP assay, combined with the use of pharmacological inhibitors, was used to examine the endocytic pathways involved in NP uptake. We determined that pHlexi NPs were internalized primarily via a dynamin-dependent pathway. The SHIP assay allows high-throughput analysis of cells and is amenable to a wide range of NP systems. This study demonstrates the SHIP assay is a valuable tool in obtaining greater understanding of NPs behavior with cells, which is an important step in designing better delivery systems.

## **MATERIALS AND METHODS**

**Materials** 2-(diethylamino) ethyl methacrylate (DEAEMA) (Sigma-Aldrich, 99%) and poly(ethylene glycol methacrylate) (PEGMA) (Sigma-Aldrich, average  $M_n$  300 Da) were passed over aluminium oxide (activated, basic) (Sigma-Aldrich) to remove inhibitors prior to use. 4-Cyano-4-[(dodecylsulfanyl thiocarbonyl) sulfanyl] pentanoic acid (Sigma-Aldrich, 97%) and all solvents were used as received. PDEAEMA (~36 kDa) was synthesized as previously described(9). Cyanine5 amine was purchased from Lumiprobe. FIP<sub>DBCO</sub> (5' Cy5-TCAGTTCAGGACCCTCGGCT-DBCO 3') was purchased from IBA, USA. QP<sub>C</sub> (5' AGCCGAGGGTCCTGAACTGA-BHQ2 3') and

QP<sub>M</sub> (GCGTCCATCTCATTTCAGCGT-BHQ2 3') were purchased from Integrated DNA Technologies, USA. Human holo-transferrin (Tf) was purchased from Sigma-Aldrich and functionalized with FIP as previously described(6). Dyngo-4a (Abcam) and 5-(N-ethyl-N-isopropyl) amiloride (EIPA; Sapphire Biosciences) were aliquoted in dimethyl sulfoxide (DMSO) and phosphate buffered saline (PBS) to final concentrations of 0.5 mM and 1 mM respectively. Sodium azide was dissolved in PBS to a final concentration of 2.4 M.

**Cell culture** 3T3 mouse embryonic fibroblast wild type cells (3T3 MEFs WT, ATCC CRL-2752) were cultured in DMEM medium supplemented with 10% fetal bovine serum, 100 U mL<sup>-1</sup> penicillin and 100 µg mL<sup>-1</sup> streptomycin. CEM human T lymphoblast cells (CCRF-CEM, ATCC CCL-119) were cultured in RPMI-1640 medium supplemented with 10% fetal bovine serum, 2 mM L-Glutamine, 1% sodium pyruvate, 1% MEM non-essential amino acids, 100 U mL<sup>-1</sup> penicillin and 100 µg mL<sup>-1</sup> streptomycin. For fluorescence imaging, 3T3 MEFs WT cells were seeded at 4.0 x 10<sup>4</sup> cells per well in 8 well chamber slides. For viability assays 3T3 MEFs WT cells were seeded at 1.0 x 10<sup>4</sup> cells per well in 96-well plates and incubated overnight (37°C and 5% CO<sub>2</sub>). CEM cells were seeded at 1.5 x 10<sup>4</sup> cells per well in 96-well plates on the day of the experiment. For all flow cytometry experiments (internalization kinetics and inhibitor studies) 3T3 cells were seeded at 6.0 x 10<sup>4</sup> cells per well in 24-well plates and incubated overnight (37°C and 5% CO<sub>2</sub>). CEM cells were seeded at 9.0 x 10<sup>4</sup> cells per well in 24-well plates on the day of the experiment. 3T3 cells were seeded at a lower density than CEM cells to allow for cell proliferation during the overnight incubation. For inhibitors studies on transferrin, cell medium was replaced with FBS free medium.

**Instruments** NMR spectra were recorded on a 400 MHz Bruker NMR using the residual proton resonance of the solvent ( $\text{CDCl}_3$  or  $\text{D}_2\text{O}$ ) as the internal standard. Aqueous phase GPC was performed on a Shimadzu liquid chromatography system equipped with a Shimadzu RID-10A detector ( $\lambda = 658 \text{ nm}$ ), using three ultrahydrogel guard columns in series (200 Å porosity, 6  $\mu\text{m}$  diameter bead size, 6 mm x 40 mm), operating at room temperature. The eluent was Milli-Q water containing 20% v/v acetonitrile and 0.1% w/v TFA at a flow rate of  $0.5 \text{ mL min}^{-1}$ . Nanoparticle size and polydispersity measurements were performed on a Horiba nanopartica SZ-100 (Horiba Scientific, Japan) operating at a fixed scattering angle of  $90^\circ$ . The zeta potential was determined using a Malvern Zetasizer (Malvern Instruments, Worcestershire, UK). Flow cytometry studies (internalization kinetics and inhibitor studies) were performed on a S100EXi flow cytometer (Stratedigm).

**Synthesis of poly(poly(ethylene glycol methacrylate)) (PEGMA) macro RAFT agent** Poly(ethylene glycol methacrylate) (PEGMA; average  $M_n$  300 Da) (2.71 g, 9.03 mmol), AIBN (0.93 mg, 6.0  $\mu\text{mol}$ ) and 4-cyano-4-[(dodecylsulfanylthiocarbonyl)sulfanyl] pentanoic acid (20.7 mg, 51.3  $\mu\text{mol}$ ) were dissolved in 1,4-dioxane (7.4 g) and placed into a Schlenk flask with a magnetic stirrer bar. The flask was degassed over three freeze-pump-thaw cycles. The reaction mixture was stirred in an oil bath at  $60^\circ\text{C}$  for 16 h. The reaction was terminated by exposure to air. The polymer was purified by precipitation from cold hexane twice and dried under reduced pressure. The molecular weight of the polymer was determined by  $^1\text{H}$  NMR to be approximately 11 kDa.  $^1\text{H}$ -NMR (400 MHz;  $\text{CDCl}_3$ ):  $\delta$  4.07 (-COO- $\text{CH}_2$ - $\text{CH}_2$ -), 3.65 (PEG backbone), 3.54 (-COO- $\text{CH}_2$ - $\text{CH}_2$ -), 3.37 (-O-

$CH_3$ ), 1.90-1.75 (backbone  $-CH_2-C-CH_3-$ ), 1.24 ( $CH_3-C_8H_{16}-CH_2-$ ), 1.05-0.82 (backbone  $-CH_2-C-CH_3-$ ).

**Synthesis of poly(poly(ethylene glycol methacrylate)-*b*-2-(diethylamino) ethyl methacrylate) (PEGMA-*b*-PDEAEMA)** DEAEEMA(367 mg, 2.0 mmol), AIBN (0.3 mg, 1.8  $\mu$ mol) and PEGMA<sub>37</sub> macro-RAFT agent (200 mg, 18  $\mu$ mol) were dissolved in 1,4-dioxane (1.6 g) and placed into a Schlenk flask with a magnetic stirrer bar. The reaction mixture was stirred in an oil bath at 60°C for 16 h. The reaction was terminated by exposure to air. The polymer was purified by dialysis in PBS pH 6, followed by Milli-Q water (12 kDa membrane) and the product was lyophilized. The molecular weight of the PDEAEMA was determined by <sup>1</sup>H NMR to be approximately 17 kDa. <sup>1</sup>H NMR (400 MHz; D<sub>2</sub>O):  $\delta$ /ppm: 4.40 (PDEAEMA -COO- $CH_2-CH_2-$ ), 4.18 (PEGMA -COO- $CH_2-CH_2-$ ), 3.79 (PEG), 3.64 (PEGMA-COO- $CH_2-CH_2-$ ), 3.55 ( $-CH_2-CH_2-N-$ ), 3.40 ( $-O-CH_3$ ), 3.32 ( $-N-CH_2-CH_3$ ), 1.98 (backbone  $-CH_2-C-CH_3-$ ), 1.33 ( $-N-CH_2-CH_3$ ), 1.08 (backbone  $-CH_2-C-CH_3-$ ).

**Synthesis of pentafluorophenyl methacrylate** Pentafluorophenol (5.0 g, 2.7 mmol), triethylamine (4.1 g, 41 mmol) and 4-dimethylaminopyridine (DMAP; 0.67 g, 27 mmol) were dissolved in dry dichloromethane (DCM; 30 mL). Nitrogen was bubbled through the solution for 5 min at 0°C. Methacrylic anhydride (6.1 mL, 41 mmol) was added slowly via a syringe with vigorous stirring. The resulting solution was stirred at room temperature for 12 hours under a nitrogen atmosphere. The solution was diluted with DCM (20 mL) and washed with 0.1 M HCl (50 mL), water (50 mL) and brine (50 mL). The organic layer was dried over MgSO<sub>4</sub>, filtered and concentrated *in vacuo*. The crude product was purified by automated column chromatography

(Reveleris X2 Flash Chromatography System, Grace, USA) with a gradient of *n*-hexane and ethyl acetate to give pentafluorophenol methacrylate as a colourless liquid (4.2 g, 61%).  $^1\text{H}$  NMR (400 MHz;  $\text{CDCl}_3$ ):  $\delta/\text{ppm}$ : 6.45 (quintet,  $J = 1$  Hz), 5.91 (qd,  $J = 1.6, 1.3$  Hz), 2.09 (dd,  $J = 1.6, 1.0$  Hz);  $^{19}\text{F}$  NMR (376 MHz;  $\text{CDCl}_3$ ):  $\delta/\text{ppm}$ : -152.77 (d, 2F,  $J = 16$  Hz, *ortho*), -158.17 (1F, t,  $J = 22$  Hz, *para*), 162.46 (2F, dd,  $J = 16, 22$  Hz, *meta*).

**Synthesis of poly(2-(diethylamino)ethyl methacrylate-*r*-pentafluorophenyl methacrylate) p(DEAEMA-*r*-PFPMA)** DEAEMA (1.0 g, 5.4 mmol), PFPMA (14 mg, 5.5  $\mu\text{mol}$ ), AIBN (0.2 mg, 1.1  $\mu\text{mol}$ ) and 4-Cyano-4-[(dodecylsulfanylthiocarbonyl)sulfanyl]pentanoic acid (4.4 mg, 11  $\mu\text{mol}$ ) were dissolved in 1,4-dioxane (1.0 g) and placed into a Schlenk flask with a magnetic stirrer bar. The flask was degassed over three freeze-pump-thaw cycles. The reaction mixture was stirred in an oil bath at 60°C for 18 h. The reaction was terminated by cooling and exposing the reaction mixture to air. The polymer was precipitated in water, dissolved in DCM and dried over  $\text{MgSO}_4$  to prevent hydrolysis of the PFP ester. The polymer was further purified by precipitation in cold *n*-hexane. The precipitate was dried *in vacuo* to give P(DEAEMA-*r*-PFPMA) as a tacky solid. The molecular weight of the polymer was determined by  $^1\text{H}$  (DEAEMA) and  $^{19}\text{F}$  (PFPMA) NMR analysis to be approximately 49 kDa with 4 PFP esters per chain.  $^1\text{H}$  NMR (400 MHz;  $\text{CDCl}_3$ ):  $\delta/\text{ppm}$ : 3.99 (-COO- $\text{CH}_2$ - $\text{CH}_2$ -), 2.69 (- $\text{CH}_2$ - $\text{CH}_2$ -N-), 2.56 (-N- $\text{CH}_2$ - $\text{CH}_3$ ), 1.90,-1.78 (backbone - $\text{CH}_2$ -C- $\text{CH}_3$ -), 1.26 ( $\text{CH}_3$ - $\text{C}_8\text{H}_{16}$ - $\text{CH}_2$ -), 1.03 (-N- $\text{CH}_2$ - $\text{CH}_3$ ), 0.88 (backbone - $\text{CH}_2$ -C- $\text{CH}_3$ -);  $^{19}\text{F}$  NMR (376 MHz;  $\text{CDCl}_3$ ):  $\delta/\text{ppm}$ : -149.27 (1F, *ortho*), -151.35 (1F, *ortho'*), -157.83 (1F, *para*), -162.11 (2F, *meta*).

**Modification of p(DEAEMA-r-PFPMA) with FIP** P(DEAEMA-r-PFPMA) (20 mg, 1.3  $\mu\text{mol}$  PFP ester groups) was dissolved in 1 mL of acetonitrile. Azido-PEG<sub>3</sub>-Amine (0.55 mg, 2.5  $\mu\text{mol}$ ) and triethylamine (1  $\mu\text{l}$ , 6.6  $\mu\text{mol}$ ) were added. The reaction was stirred at 50°C for 48 h. <sup>19</sup>F NMR was performed on the crude reaction to determine coupling efficiency. The polymer was purified by dialysis in PBS pH 6, followed by Milli-Q water (12 kDa membrane) and the product was lyophilized. FIP<sub>DBCO</sub> was added at 0.0125 molar equivalents to PFPMA ester groups (approximately one DNA molecule per 20 polymer chains) in PBS pH 6 (at final polymer concentration of 2 mg mL<sup>-1</sup>) and stirred at RT for 6 h. The sample was run on a 2% agarose gel to confirm the conjugation was successful.

**Modification of p(DEAEMA-r-PFPMA) with Cy5** P(DEAEMA-r-PFPMA) (20 mg, 1.3  $\mu\text{mol}$  PFP ester groups) was dissolved in 1 mL of acetonitrile. Cy5 amine (0.5 mg, 0.82  $\mu\text{mol}$ ) and triethylamine (1  $\mu\text{l}$ , 6.6  $\mu\text{mol}$ ) were added. The reaction was stirred at 50°C for 48 h. The polymer was purified by dialysis in PBS pH 6, followed by Milli-Q water (12 kDa membrane) and the product was lyophilized.

**Synthesis of FIP functionalized PDEAEMA pHlexi nanoparticles** FIP-PDEAEMA and PEGMA-b-PDEAEMA were co-dissolved into 3 mL PBS (pH 6) to a total mass of 3 mg such that the total PEGMA content was 5% (w/w). The polymer mixture was dialyzed overnight against PBS pH 8 in 3.5 kDa MWCO dialysis devices to gradually increase the pH. The resulting particles were purified by further dialysis against PBS pH 8 in 100 kDa MWCO dialysis devices. The buffer was changed six times over a 24-hour period. The NP solution was removed from dialysis and left to sit for 24

hours. The particles were filtered with a 0.45  $\mu\text{m}$  polyethersulfone (PES) filter immediately prior to any experiments.

**Cryo-Electron Microscopy (cryo-EM)** Samples were prepared on 200-mesh copper grids coated with perforated carbon film (Lacey carbon film: ProSciTech, Qld, Australia) and frozen in liquid ethane. The samples were examined using a Gatan 626 cryoholder (Gatan, Pleasanton, CA, USA) and Tecnai 12 Transmission Electron Microscope (FEI, Eindhoven, The Netherlands) at an operating voltage of 120 kV. At all times low dose procedures were followed, using an electron dose of 8-10 electrons/ $\text{\AA}^2$ . Images were recorded using a FEI Eagle 4kx4k CCD camera.

**Alamar Blue viability assay** FIP-NPs were added to 3T3 or CEM cells at various concentrations in triplicate and incubated for 4 hours at cell culture conditions (37°C and 5%  $\text{CO}_2$ ). The media was replaced with fresh media containing 10  $\mu\text{l}$  Alamar Blue reagent and incubated for a further 4 hours. Fluorescence was measured on a FLUOstar OPTIMA microplate reader (Excitation 510 nm, Emission 610 nm; BMG Labtech, Germany). Viability was calculated as the percent of fluorescence relative to untreated control cells.

**Live cell fluorescence microscopy** Live cell imaging was performed using an Olympus IX83 microscope with a 60x 1.3 NA silicone objective (with a standard “Pinkel” DAPI/FITC/CY3/CY5 filter set from Semrock). The cells were imaged in a humidified incubation chamber with 10%  $\text{CO}_2$  at 37 °C. Images were taken as a series of z-sections with 0.33 mm spacing and deconvolved using the Richardson–Lucy

algorithm (100 iterations).(15, 16) All images were processed using the Slidebook 6.0 software.

*Internalization:* FIP-NPs ( $1 \mu\text{g mL}^{-1}$ ) were added to 3T3 cells and incubated for 4 hours ( $37^\circ\text{C}$  and  $5\% \text{CO}_2$ ). Cells were washed once in FuoroBrite DMEM (Life Technologies) and incubated with wheat germ agglutinin Alexa Fluor 488 conjugate ( $5 \mu\text{g mL}^{-1}$ ; Life Technologies) for a further 10 min. Cells were washed two times in FuoroBrite DMEM and imaged in medium containing Hoescht nuclear stain ( $2.5 \mu\text{g mL}^{-1}$ ; Life Technologies) and sodium azide (100 mM). During imaging QP<sub>c</sub> ( $1 \mu\text{M}$ ) was added.

*Localization:* 3T3 MEFs WT cells were seeded in an 8 well chamber slide and late endosomes/lysosomes were labelled using CellLight Lysosomes-GFP and BacMam enhancer (Life Technologies) according to manufacturer's instructions. FIP-NPs ( $1 \mu\text{g mL}^{-1}$ ) were added to the cells and incubated for 4 h. The cells were washed 3 times in PBS, and FluoroBrite imaging media (Thermo Fisher Scientific) containing Hoeschst stain (Thermo Fisher Scientific,  $2.5 \mu\text{g mL}^{-1}$ ) was added and incubated for 5 minutes before imaging.

**Internalization kinetics of PDEAEMA pHlexi nanoparticles** FIP-NPs ( $1 \mu\text{g mL}^{-1}$  in 3T3 or  $0.5 \mu\text{g mL}^{-1}$  in CEM) were added to the cells in triplicate at various time-points. 3T3 cells were washed twice in PBS, lifted with trypsin and split into two for quenched/non-quenched samples, followed by two more washes in 1% BSA. As CEM cells are non-adherent they were immediately split into two and washed four times in 1% BSA. All samples were re-suspended in PBS containing propidium iodide (PI;  $0.5 \mu\text{g mL}^{-1}$ ) with or without QP<sub>c</sub> ( $1 \mu\text{M}$ ) for analysis by flow cytometry. The percent positive cell population was calculated using our HD flow deconvolution algorithm

(manuscript submitted) and the mean fluorescence intensity (MFI) was determined from the positive cell population. Percent of internalized NPs was calculated as the MFI ratio of quenched samples versus unquenched samples. The experiment was performed at least 3 times in triplicate.

### **Inhibitor studies**

Cells were incubated with Dyngo-4a (25  $\mu\text{M}$ ), EIPA (50  $\mu\text{M}$ ) or  $\text{NaN}_3$  (120 mM) for 15 min. FIP-NPs (1  $\mu\text{g mL}^{-1}$  in 3T3 or 0.5  $\mu\text{g mL}^{-1}$  in CEM) and calcein (100  $\mu\text{g mL}^{-1}$ ) were added to the cells and incubated for 1 hour. FIP-Tf (0.3  $\mu\text{g mL}^{-1}$ ) was added to cells (in FBS free medium) and incubated for 1 hour. After incubation, 3T3 cells were washed twice in PBS, lifted with trypsin and split into two for quenched/non-quenched samples, followed by two more washes in 1% BSA. CEM cells were immediately split into two and washed four times in 1% BSA. Quenched samples were placed on ice until analysis. All samples were re-suspended in PBS containing PI (0.5  $\mu\text{g mL}^{-1}$ ) with or without  $\text{QP}_C$  (1  $\mu\text{M}$ ) for analysis by flow cytometry. The experiment was performed at least 3 times in triplicate.

## **RESULTS**

### **FIP-NP Synthesis and Characterization**

To perform the SHIP assay, first it was necessary to incorporate the FIP sensor into the polymeric NPs. FIP can be attached to NPs through a variety of coupling strategies, including biotin/avidin coupling, amine/succinimidyl ester chemistry, thiol/malaimide coupling and azide/alkyne click chemistry. We chose azide/alkyne click chemistry as it enables rapid coupling without unwanted side reactions(17). Cy5 modified FIP was custom synthesized with a strained cyclo-octyne

(dibenzocyclooctyl - DBCO) group on the 3' end to enable copper free coupling to an azide group on the NPs. Azide groups were incorporated into the NP through a two step process by first copolymerizing the PDEAEMA with pentafluorophenyl methacrylate (PFPMA). The pentafluorophenyl (PFP) group is an activated ester that reacts efficiently with primary amines and has been widely used as a post-polymerization modification strategy to incorporate functional groups that cannot be incorporated via direct polymerization(18, 19). The polymer was modified with an azide by reacting the PFP groups with an azido-PEG<sub>3</sub>-amine linker (Scheme 1). This reaction went to 70% completion as determined by <sup>19</sup>F NMR (Fig. S4). The polymer was dialyzed in PBS pH 6 followed by Milli-Q water to protonate the PDEAEMA into the water-soluble form. The FIP<sub>DBCO</sub> was then clicked onto the azide modified PDEAEMA polymer and conjugation was verified by gel electrophoresis. All of the FIP was conjugated to the polymer as the FIP conjugated PDEAEMA remained in the well, whereas free FIP migrated down the gel (Fig. S5).

The two polymeric components, FIP-PDEAEMA and PEGMA-b-PDEAEMA, were co-dissolved (at a ratio such that the overall PEGMA content was 5% w/w) into phosphate buffered saline (PBS; pH 6) and dialyzed against PBS at pH 8 to induce particle formation. The polymers self-assemble into nanoparticles as the pH responsive PDEAEMA component shifts from the hydrophilic form at pH 6 into the hydrophobic form at pH 8 as the polymer becomes deprotonated above its pKa(9). The mean diameter of the nanoparticles was determined to be  $155 \pm 4$  nm by dynamic light scattering measurements (Fig. 1a) with a polydispersity index of 0.06 indicating a narrow size distribution. FIP-NPs showed a slightly negative zeta potential of  $-2.8 \pm 0.3$  mV. Unmodified NPs synthesized by the same method (using un-labeled

PDEAEMA homopolymer) showed no significant difference in size, polydispersity or zeta-potential (Table. S2). Cryo electron microscopy (cryo-EM) images of the FIP-functionalized NPs show spherical particles of approximately 150 nm, consistent with results from DLS (Fig. 1b). To confirm the FIP was still functional when attached to the NPs, the complementary quencher probe (QP<sub>C</sub>) was added to the particles. Efficient quenching of the Cy5 signal was observed by fluorescence spectroscopy, whereas no significant quenching was observed using a mismatched quencher sequence (QP<sub>M</sub>; Fig. 1c).

### **Nanoparticle Internalization Kinetics**

To demonstrate the SHIP assay works efficiently *in vitro*, we incubated the FIP-NPs with 3T3 cells for 4 hours. To highlight the cell membrane, the cells were stained with wheat germ agglutinin. Figure 2 shows the maximum intensity projection of a Z-stack of the cells (a) before and (b) after the addition of QP<sub>C</sub>. A comparison of the two images shows the fluorescence from a number of the nanoparticles is quenched after the addition of QP<sub>C</sub>, indicating they are on the surface of the cell.

To test the internalization kinetics of the NPs into 3T3 and CEM cells, FIP-NPs were incubated with cells for 0.5, 1, 2, 4 or 6-hours. The concentration of FIP-NPs after filtration was first determined by UV-vis spectroscopy using the absorbance of the Cy5 (649 nm; Fig. S6). NP concentrations were chosen based on cell viability in both cell lines as measured by the Alamar Blue assay (Fig. S7). The samples were split equally into two samples, and QP<sub>C</sub> was added to one sample immediately before analysis by flow cytometry. The unquenched sample was used to determine the percent of cells with NPs associated, and the ratio of the MFI of the quenched sample divided by the MFI of the unquenched sample, was used to determine the percent of

the nanoparticles that were internalized into the cells. For all samples, cell viability was >80% as measured by PI staining (data not shown).

The percent of cells with NPs associated was similar for both cell lines. The association of NPs with 3T3 cells was 84% after 30 min and increased to 98% after 4 hours (Fig. 3a). In CEM cells, the association plateaued after 30 min (with 99% of the cells being associated with NPs; Fig. 4a). The pattern of NP internalization differed significantly between the two cell lines. In 3T3 cells the amount of associated NPs continued to increase up to 2 hours as shown by the MFI of the cells positive for NP association (Fig. 3b). Internalization of membrane-associated NPs occurred rapidly within the first hour of incubation with the 3T3 cells, with 66% of the associated NPs internalized within an hour, and 89% of the particles internalized after 6 hours (Fig. 3c). NP association with CEM cells plateaued after 1 hour (Fig. 4b). CEM cells showed significantly decreased internalization compared to 3T3 cells, showing maximum internalization after 30 min (20%; Fig. 4c).

To assess cellular localization of the endocytosed NPs, FIP-NPs were incubated with 3T3 cells expressing GFP-tagged lysosomal associated membrane protein 1 (LAMP1). The NPs were co-localized with LAMP1 (Fig. 5).

### **Mechanism of Internalization**

To investigate the role of specific endocytic pathways in the internalization of NPs, the 3T3 and CEM cell lines were treated with a range of inhibitors: NaN<sub>3</sub>, to inhibit all energy dependent internalization pathways, Dyngo-4a, to inhibit dynamin dependent pathways, and EIPA, to inhibit macropinocytosis. Cells were treated with inhibitor 15 min prior to addition of the NPs. The NPs were incubated with the cells for 1 hour, in order to allow sufficient time for detectable levels of NPs to enter cells,

without inducing toxicity. Propidium iodide (PI) staining was used to validate that minimal cell damage had occurred after treatment with inhibitors at the concentrations used for each cell line. In all cases >80% viability was observed (Fig. S8). The SHIP assay was then used to distinguish internalized NPs from NPs bound to the cell surface. The effects of the inhibitors used in this study on the main internalization pathways are summarized in Fig. 6a. There are a number of potential limitations with the use of internalization inhibitors: 1) Inhibitors may be non-specific and inhibit multiple pathways(20); 2) The inhibition of internalization may be indicative of cell stress and not inhibition of a specific pathway; and 3) if the concentration of inhibitor is not high enough, then the lack of inhibition may be interpreted as the pathway not being involved with internalization. To control for these limitations we incubated the cells with calcein, a small membrane impermeable fluorophore that is known to be endocytosed via macropinocytosis, and human transferrin (Tf), which is internalized via clathrin dependent endocytosis(21). The internalization of NPs was compared to these controls.

$\text{NaN}_3$  (120 mM) was used to inhibit all energy-dependent internalization pathways, and resulted in a strong decrease in NP internalization in both cell types (87% in 3T3; 82% in CEM; Fig. 6b and S9), calcein (>40%; Fig. S10) and Tf (>80%; Fig. S11 and S12). Inhibition of the dynamin-dependent pathways by Dyngo-4a (30  $\mu\text{M}$ ) reduced internalization of NPs in 3T3 by 92%. A strong reduction of Tf uptake (>55%) was observed in Dyngo-4a treated cells (Fig. S11 and S12). The uptake of calcein was not significantly affected by the presence of Dyngo-4a (Fig. S10).

Macropinocytosis was inhibited with EIPA (50  $\mu$ M) and resulted in a 53% decrease in NP internalization in 3T3 cells, however no inhibitory effect in CEM cells was observed (Fig. 6 and S9). Calcein internalization was inhibited by EIPA in 3T3 cells (>40%), however similar to the NPs, EIPA did not inhibit calcein internalization in CEM cells (Fig. S9). EIPA did not inhibit the internalization of Tf in either cell line (Fig. S11 and S12).

## **DISCUSSION**

Understanding the internalization of NPs into cells is of great importance to enable engineering of better drug delivery systems. If NPs simply bind to the surface of the cell without being internalized, many of the advantages of using NP mediated delivery are negated. Internalization is governed by a number of factors relating to the physicochemical properties of the particle and the different types of cell(22). In order to study internalization effectively, high-throughput assays to distinguish between membrane association and internalization of materials are required. In this study we demonstrate the use of the SHIP assay to study the internalization kinetics of NPs, and map the differences in uptake of two different cell lines. We have also combined the SHIP assay with chemical inhibitors to gain insight into the mechanisms of internalization. Modification of the NPs with FIP did not significantly alter the assembly or size of the NPs, compared with NPs synthesized from similar polymers without the FIP. Cryo-EM images of the FIP NPs (Figure 1b) appear similar to non-functionalized NPs that we have previously imaged(9), indicating that functionalization of the nanoparticle surface with the FIP probe does not affect the NP size or morphology. >99% quenching was achieved when the QP<sub>C</sub> was added to the FIP NPs, which demonstrates the FIP is accessible to the quencher (Figure 1c). QP<sub>C</sub>

also effectively quenches FIP NPs bound to the surface of the cell *in vitro* as shown in Figure 2. The internalized NPs showed no significant quenching, demonstrating the utility of the SHIP assay for quantifying internalization of NPs.

We chose two significantly different cell lines to highlight differences in NP internalization behavior. 3T3 cells are an adherent mouse fibroblast cell line and CEM cells are a suspension human T-lymphoblast. Co-localization of FIP-NPs with LAMP1 lysosomal stain suggests that the NPs are endocytosed and trafficked to the lysosomes (Figure 5). This is consistent with our previous observations that unmodified NPs are confined to the lysosomes after internalization(9).

Using the SHIP assay, the kinetics of association and internalization were analyzed by flow cytometry and found to differ significantly between the two cell types studied. The SHIP assay gives four key pieces of information that help to understand the behavior of the NPs. The percent of cells with nanoparticles associated gives information about the interactions of NPs with the global population of cells. The MFI of the cells that have particles bound illustrates the average number of particles that are associated with each cell. The MFI of the quenched samples gives information about the average number of particles that have been internalized, and finally, the ratio of the quenched MFI to the un-quenched MFI measures the percent of NPs that have been internalized.

NPs showed rapid association with both 3T3 and CEM cells, with more than 90% of the cells having nanoparticles associated after 1 hour. The MFI of the 3T3 cells gradually increased with time, indicating increasing association of nanoparticles

with cells. The fluorescence of the quenched sample also increased with time, suggesting the 3T3 cells rapidly internalize the NPs once the NPs bind to the cell surface. After 6 hours, ~90% of the NPs bound to the cells were internalized. In contrast, only ~20% of the NPs bound to CEM cells were internalized. While the MFI of the CEM cells was similar to the MFI of the 3T3 cells after 1 hour, the MFI of the CEM cells only increased 12% over 6 hours in CEM cells compared to 44% in 3T3 cells. This suggests that while the initial interaction of NPs with CEM and 3T3 cells is similar, the association between CEM cells and NPs does not increase significantly over time. The MFI of the quenched CEM cells showed significantly decreased internalization compared to 3T3 cells, with no significant increase in the percent of NPs internalized over time. This suggests that after the initial binding of the NPs to the CEM cells, the NPs remain on the surface of the cell and are not internalized. NPs bound to the surface of the CEM cell saturate the available binding sites and prevent further association of NPs to the cells, thus the MFI of the cells remains constant. In 3T3 cells, when NPs are internalized into the cells, the space on the surface of the cell is free to bind additional NPs, therefore the MFI of the cells increases with time.

The association and internalization results show significant differences in cell behavior between the two cell lines, so we next investigated the mechanism by which the NPs are internalized into the cells. To compare NP internalization with known internalization pathways, Tf and calcein were used as controls that exhibit dynamin-dependent endocytosis and macropinocytosis respectively. Tf was functionalized with FIP to quantify internalization, however, as calcein should not bind to the cell surface, we determined calcein internalization by simply washing the excess calcein from the cells.  $\text{NaN}_3$  inhibits all energy dependent endocytosis pathways and effectively

inhibited internalization of NPs, calcein and Tf in both cell lines. This is indicative of active uptake of the NPs via an energy dependent process. This verifies the SHIP assay can be used to probe endocytosis by small molecule inhibitors.

The cells were incubated with calcein and NPs simultaneously. Dyngo-4a induced strong inhibition of NP internalization in 3T3 cells (92% inhibition). Calcein, which is known to be internalized by macropinocytosis was not inhibited by the Dyngo-4a but was inhibited by the macropinocytosis inhibitor EIPA (Figure S10). This strongly suggests the NPs are internalized via a dynamin dependent mechanism in 3T3 cells. Dynamin is an enzyme that is primarily known to play a role in membrane fission during clathrin-coated vesicle formation(23), but has also recently been shown to be used in some forms of clathrin-independent endocytosis, including caveolae-mediated endocytosis(24) as well as some forms of clathrin and caveolae-independent endocytosis. The percentage of NPs internalized in CEM cells was low (5%) and therefore, the inhibitors have significantly less effect on CEM cells than 3T3 cells. The different pattern of inhibition with NPs compared to calcein demonstrates distinct uptake pathways. It also suggests that internalization was not influenced by any interactions between NPs and calcein in the assay.

In comparison, EIPA inhibited NP internalization in 3T3 cells by only 53%. Ivanov *et al.* demonstrated EIPA may also block clathrin dependent internalization as well as macropinocytosis via modulation of the actin cytoskeleton(25). This suggests that while macropinocytosis may play a role in NP internalization, dynamin-dependent processes are the dominant internalization mechanism in 3T3 cells. CEM cells showed significantly lower (20%) uptake of calcein than 3T3 cells, which

suggests macropinocytosis is less active in CEM cells than 3T3 cells. Consequently, EIPA did not inhibit the internalization of either NPs or calcein in CEM cells, which suggests that macropinocytosis does not play a major role in endocytosis for CEM cells.

Interestingly, both  $\text{NaN}_3$  and Dyngo-4a reduced surface binding of NPs to CEM and 3T3 cells, while neither inhibitor significantly reduced the surface binding of Tf. Inhibition of particle binding would not be an expected side effect of endocytosis, which suggests  $\text{NaN}_3$  and Dyngo-4a affect the molecules that NPs bind to on the surface of the cell. This could be indicative of a dynamin-dependent mechanism of NP endocytosis distinct from clathrin dependent endocytosis, however further studies are required to confirm the exact pathway.

It is possible that functionalization of the NP with FIP may impact the NP interaction with cells (as with any fluorescent probe) and therefore the mechanism of uptake. To test this we used NPs where the PDEAEMA core was reacted directly with Cy5-amine via the pentafluorophenyl methacrylate. Inhibitor studies on Cy5-NPs in 3T3 cells indicated that Cy5-NP association was strongly inhibited by  $\text{NaN}_3$  and Dyngo-4a and to a lower extent by EIPA (Fig. S13). This is consistent with the results observed for FIP-NPs suggesting the FIP probe does not interfere with the internalization pathway.

## **CONCLUSION**

This study demonstrates that the FIP sensor is a powerful tool to study the uptake of NPs, enabling the high throughput investigation of particle association and internalization kinetics. By ‘clicking’ the fluorescently labelled DNA probe to the polymeric core of the NPs, the internalization was studied by specifically quenching extracellular fluorescence with a complementary quencher probe. The internalization kinetics were found to differ significantly between 3T3 fibroblast and CEM T-lymphoblast cell lines, with much higher uptake by 3T3 cells over time in comparison to CEM cells. The SHIP assay when combined with specific inhibitors also allowed the investigation of internalization pathway, a key factor governing particle behavior in a cell. It was found the pHlexi self-assembling polymeric nanoparticles used in this study were endocytosed primarily via a dynamin-dependent pathway. Understanding the endocytosis mechanism is important as it allows greater insight into the physicochemical characteristics for pathway selection as well as the investigation of the adverse effects of specific internalization pathways. This fundamental understanding has important implications for controlling cellular internalization of NP delivery systems and thus improving their efficacy to delivery therapeutic cargo. The SHIP assay is a simple and high throughput assay that has broad application in understanding cellular behavior of NPs and thus is a valuable tool for developing more effective NP delivery systems.

## **ACKNOWLEDGEMENTS**

This work was supported by the Australian Research Council through the Future Fellowship Scheme (FT120100564 – GKS and FT110100265 – APRJ) and Centre of Excellence in Convergent Bio-Nano Science and Technology (APRJ). APRJ is also

supported through the Monash University Larkin's Fellowship Scheme. We thank Lynne Waddington and Julian Ratcliffe from the CryoTEM facility, CSIRO Manufacturing Flagship.

### **Legends to Figures**

**Scheme 1.** (a) FIP functionalization of PDEAEMA via post-polymerization modification. (b) Illustration of the SHIP assay. The nanoparticle is labeled with the FIP probe. After incubation of the FIP-NPs with cells, the complementary quencher probe  $QP_C$  is added and specifically quenches fluorescence of FIP on the cell surface.

**Fig. 1** (a) Characterization of FIP-labeled nanoparticles by DLS measured in PBS pH 8. (b) Representative Cryo-electron microscopy image of FIP-labeled nanoparticles. Scale bar represents 200 nm. (c) Fluorescence measurement of NPs (Excitation 643 nm). The Cy5 fluorescence of FIP-NPs is specifically quenched by  $QP_C$ .

**Fig. 2** Fluorescence microscopy images of 3T3 MEF cells. Cells incubated with FIP-NPs (red) at 37°C for 4 hours (a) before the addition of  $QP_C$  and (b) immediately after the addition of  $QP_C$  to quench extracellular fluorescence. Cells were stained with

wheat germ agglutinin membrane stain (green) and Hoechst nuclear stain (blue). Scale bar represents 10  $\mu\text{m}$ .

**Fig. 3** Kinetics of NP internalization quantified using the SHIP assay in 3T3 cells. (a) Percent of cells with associated NPs. (b) Total signal (unquenched, red squares) and internalization (quenched, blue circles). (c) Percent of NPs internalized. (n=3, error bars represent standard deviation).

**Fig. 4** Kinetics of NP internalization quantified using the SHIP assay in CEM cells. (a) Percent of cells with associated NPs. (b) Total signal (unquenched, red squares) and internalization (quenched, blue circles). (c) Percent of NPs internalized. (n=3, error bars represent standard deviation).

**Fig. 5** Multichannel deconvolved widefield fluorescence images showing 3T3 cells incubated with FIP-NPs; (a) Cy5-labelled PDEAEMA nanoparticle fluorescence, (b) lysosomal associated membrane protein (LAMP1) staining and (c) an overlay of nanoparticle fluorescence (red) and LAMP1 late endosomal/lysosomal staining (green). The cell nucleus is stained blue with Hoechst DNA stain. Scale bar represents 10  $\mu\text{m}$ .

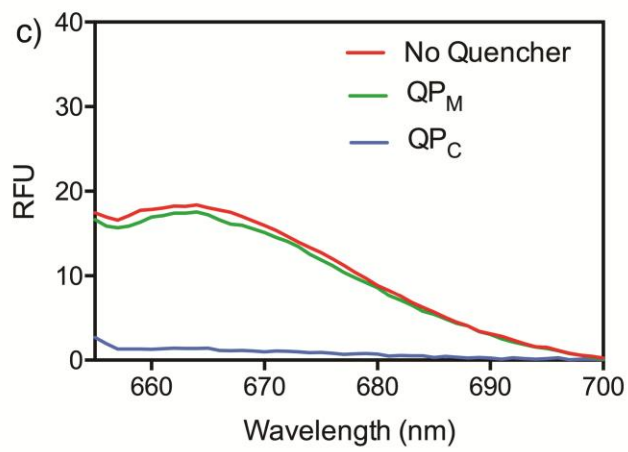
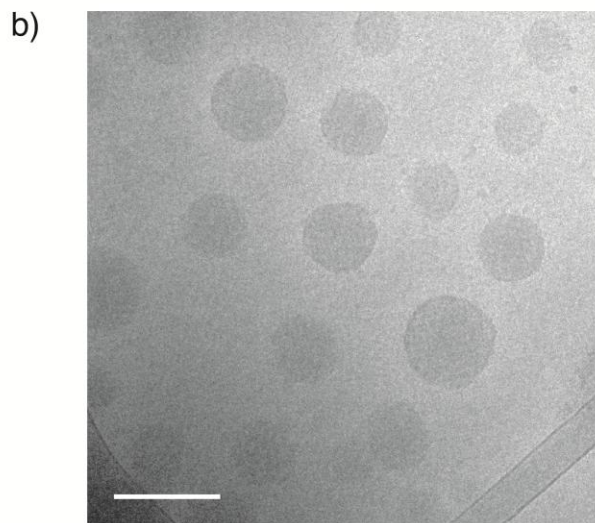
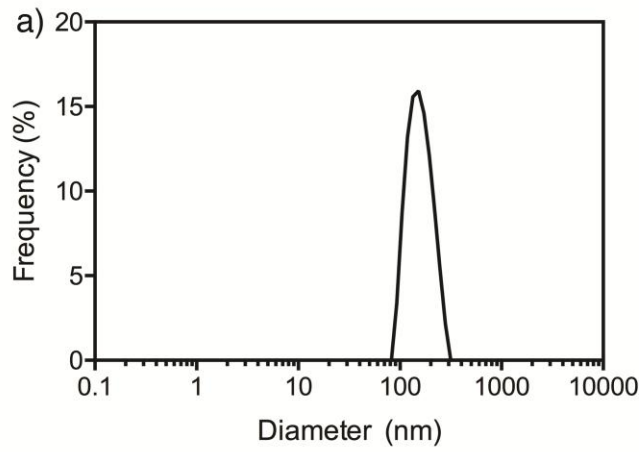
**Fig. 6** Effect of chemical inhibitors on the uptake of NPs. (a) Schematic illustration of the main endocytosis pathways and the effects of the inhibitors used in this study. (b) Flow cytometry analysis of surface associated (black) and internalized (grey) NPs after inhibition of active uptake ( $\text{NaN}_3$ ), dynamin (Dyngo-4a) and macropinocytosis (EIPA) in 3T3 cells. (c) NP internalization in 3T3 cells presented as percent of

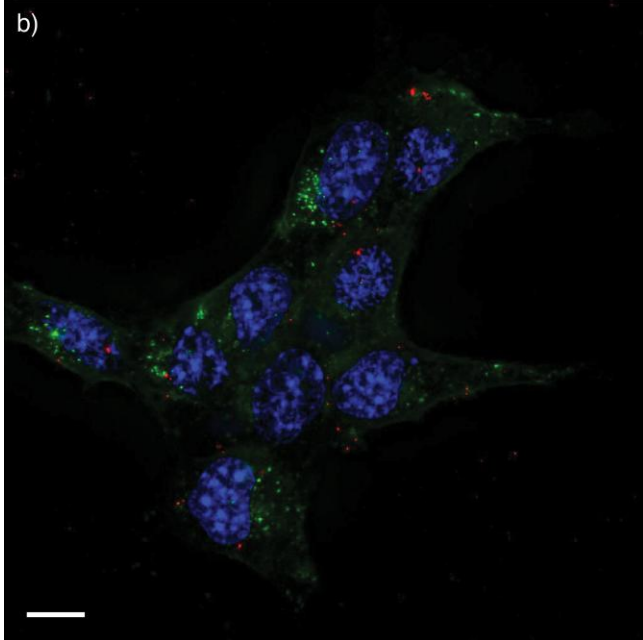
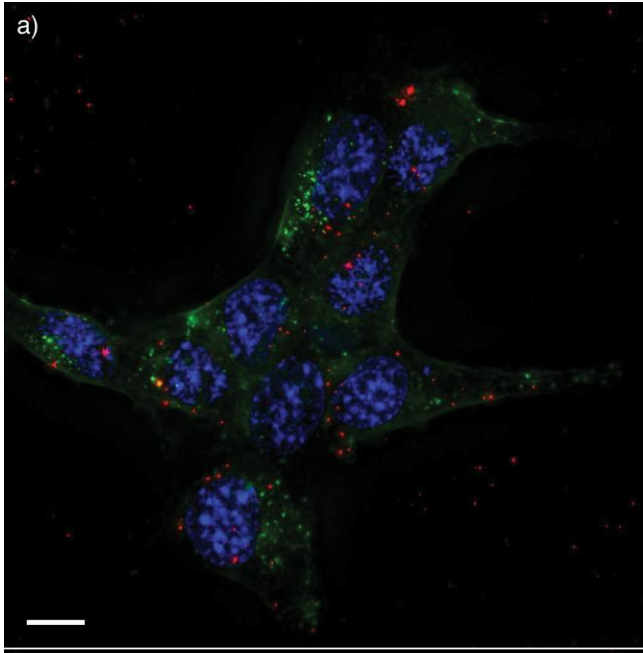
internalized NPs compared to untreated control cells. (n=3, error bars represent standard deviation).

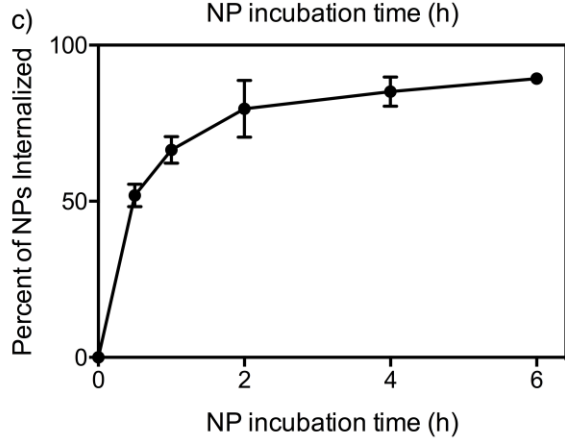
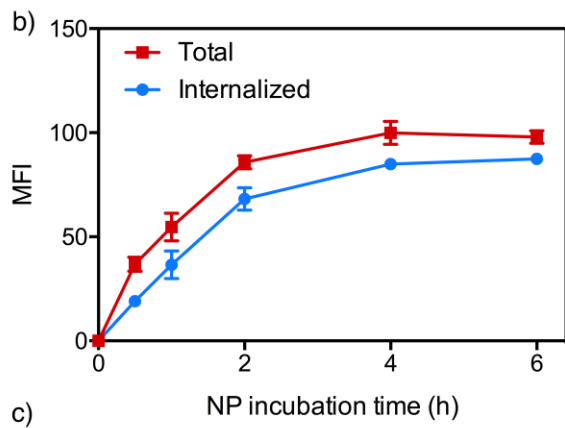
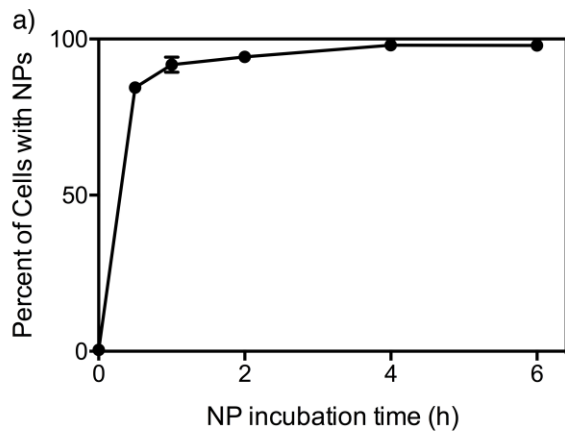
## REFERENCES

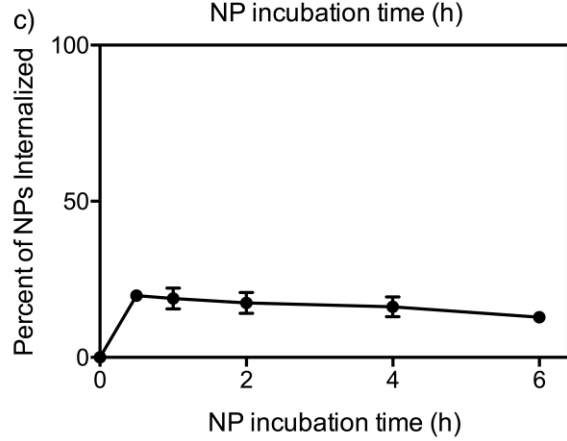
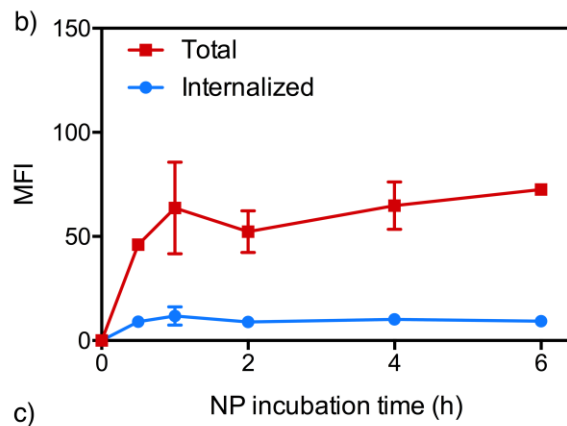
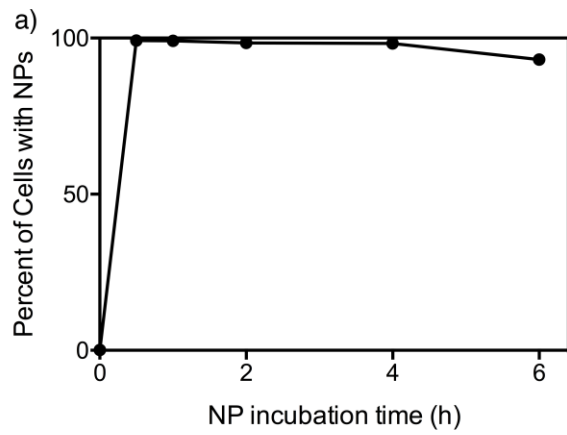
1. Johnston APR, Such GK, Ng SL, Caruso F. Challenges facing colloidal delivery systems: From synthesis to the clinic. *Current Opinion in Colloid & Interface Science*. 2011;16(3):171-81.
2. De Koker S, Hoogenboom R, De Geest BG. Polymeric multilayer capsules for drug delivery. *Chemical Society Reviews*. 2012;41(7):2867-84.
3. Rejman J, Oberle V, Zuhorn IS, Hoekstra D. Size-dependent internalization of particles via the pathways of clathrin- and caveolae-mediated endocytosis. *Biochemical Journal*. 2004;377(Pt 1):159-69.
4. Sönnichsen B, De Renzis S, Nielsen E, Rietdorf J, Zerial M. Distinct Membrane Domains on Endosomes in the Recycling Pathway Visualized by Multicolor Imaging of Rab4, Rab5, and Rab11. *The Journal of Cell Biology*. 2000;149(4):901-14.
5. Van Amersfoort ES, Van Strijp JAG. Evaluation of a flow cytometric fluorescence quenching assay of phagocytosis of sensitized sheep erythrocytes by polymorphonuclear leukocytes. *Cytometry*. 1994;17(4):294-301.
6. Liu H, Johnston APR. A Programmable Sensor to Probe the Internalization of Proteins and Nanoparticles in Live Cells. *Angewandte Chemie International Edition*. 2013;52(22):5744-8.
7. Ana-Sosa-Batiz F, Johnston APR, Liu H, Center RJ, Rerks-Ngarm S, Pitisuttithum P, et al. HIV-specific antibody-dependent phagocytosis matures during HIV infection. *Immunol Cell Biol*. 2014;92(8):679-87.
8. Reuter A, Panozza SE, Macri C, Dumont C, Li J, Liu H, et al. Criteria for Dendritic Cell Receptor Selection for Efficient Antibody-Targeted Vaccination. *The Journal of Immunology*. 2015;194(6):2696-705.
9. Wong ASM, Mann SK, Czuba E, Sahut A, Liu H, Suekama TC, et al. Self-assembling dual component nanoparticles with endosomal escape capability. *Soft Matter*. 2015;11(15):2993-3002.
10. Champion JA, Mitragotri S. Role of target geometry in phagocytosis. *Proceedings of the National Academy of Sciences of the United States of America*. 2006;103(13):4930-4.
11. Doshi N, Mitragotri S. Macrophages Recognize Size and Shape of Their Targets. *PLoS ONE*. 2010;5(4):e10051.
12. Gratton SEA, Ropp PA, Pohlhaus PD, Luft JC, Madden VJ, Napier ME, et al. The effect of particle design on cellular internalization pathways. *Proceedings of the National Academy of Sciences*. 2008;105(33):11613-8.
13. Conner SD, Schmid SL. Regulated portals of entry into the cell. *Nature*. 2003;422(6927):37-44.
14. von Kleist L, Haucke V. At the Crossroads of Chemistry and Cell Biology: Inhibiting Membrane Traffic by Small Molecules. *Traffic*. 2012;13(4):495-504.
15. Lucy LB. An iterative technique for the rectification of observed distributions. *The astronomical journal*. 1974;79:745.

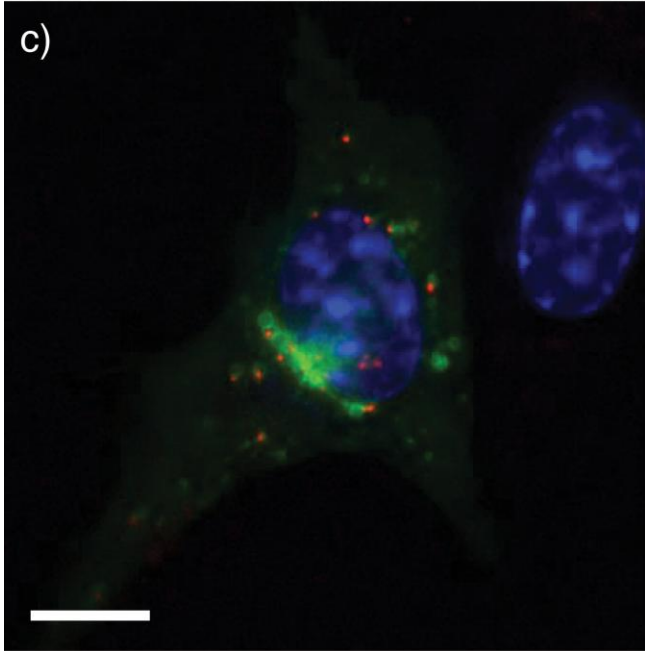
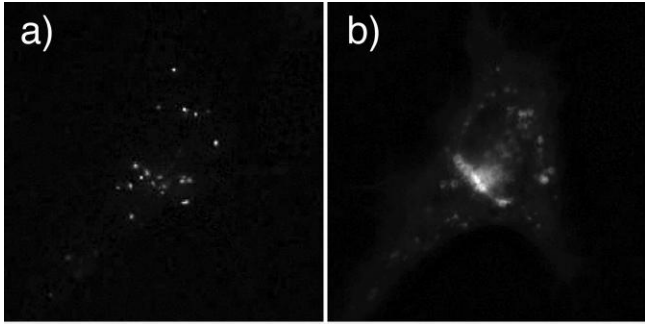
16. Richardson WH. Bayesian-Based Iterative Method of Image Restoration\*. *J Opt Soc Am.* 1972;62(1):55-9.
17. Baskin JM, Prescher JA, Laughlin ST, Agard NJ, Chang PV, Miller IA, et al. Copper-free click chemistry for dynamic in vivo imaging. *Proceedings of the National Academy of Sciences.* 2007;104(43):16793-7.
18. Eberhardt M, Mruk R, Zentel R, Théato P. Synthesis of pentafluorophenyl(meth)acrylate polymers: New precursor polymers for the synthesis of multifunctional materials. *European Polymer Journal.* 2005;41(7):1569-75.
19. Gunay KA, Schuwer N, Klok H-A. Synthesis and post-polymerization modification of poly(pentafluorophenyl methacrylate) brushes. *Polymer Chemistry.* 2012;3(8):2186-92.
20. Ivanov AI. Pharmacological Inhibition of Endocytic Pathways: Is It Specific Enough to Be Useful? In: Ivanov AI, editor. *Exocytosis and Endocytosis.* Totowa, NJ: Humana Press; 2008. p. 15-33.
21. Widera A, Norouziyan F, Shen WC. Mechanisms of TfR-mediated transcytosis and sorting in epithelial cells and applications toward drug delivery. *Advanced Drug Delivery Reviews.* 2003;55(11):1439-66.
22. Oh N, Park J-H. Endocytosis and exocytosis of nanoparticles in mammalian cells. *International Journal of Nanomedicine.* 2014;9(Suppl 1):51-63.
23. McCluskey A, Daniel JA, Hadzic G, Chau N, Clayton EL, Mariana A, et al. Building a Better Dynasore: The Dyngo Compounds Potently Inhibit Dynamin and Endocytosis. *Traffic (Copenhagen, Denmark).* 2013;14(12):1272-89.
24. Lamaze C, Dujeancourt A, Baba T, Lo CG, Benmerah A, Dautry-Varsat A. Interleukin 2 Receptors and Detergent-Resistant Membrane Domains Define a Clathrin-Independent Endocytic Pathway. *Molecular Cell.*7(3):661-71.
25. Ivanov AI, Nusrat A, Parkos CA. Endocytosis of Epithelial Apical Junctional Proteins by a Clathrin-mediated Pathway into a Unique Storage Compartment. *Molecular Biology of the Cell.* 2004;15(1):176-88.

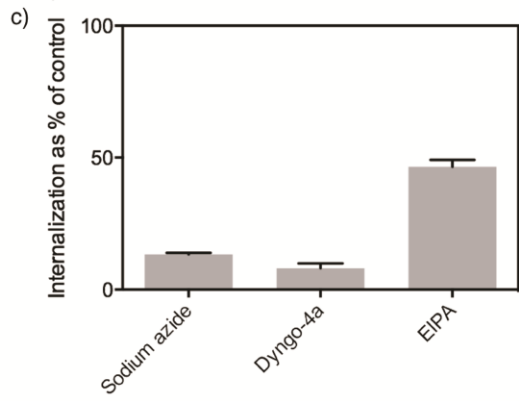
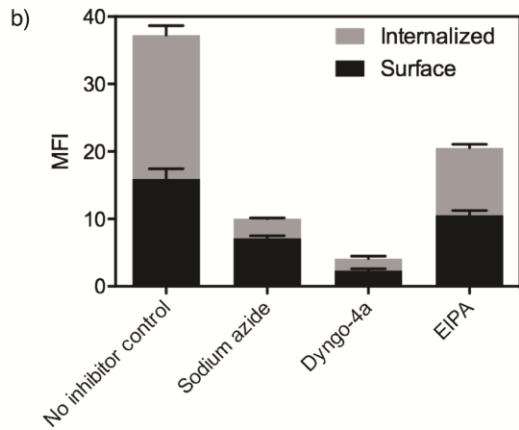
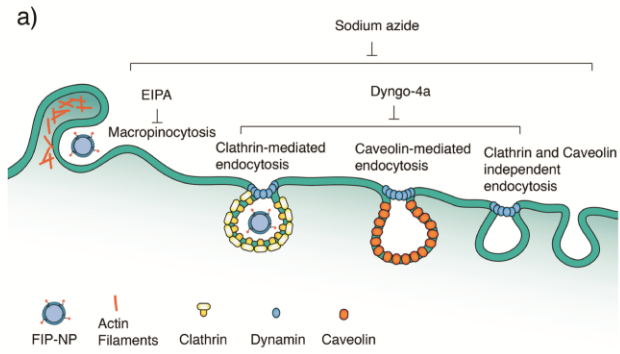


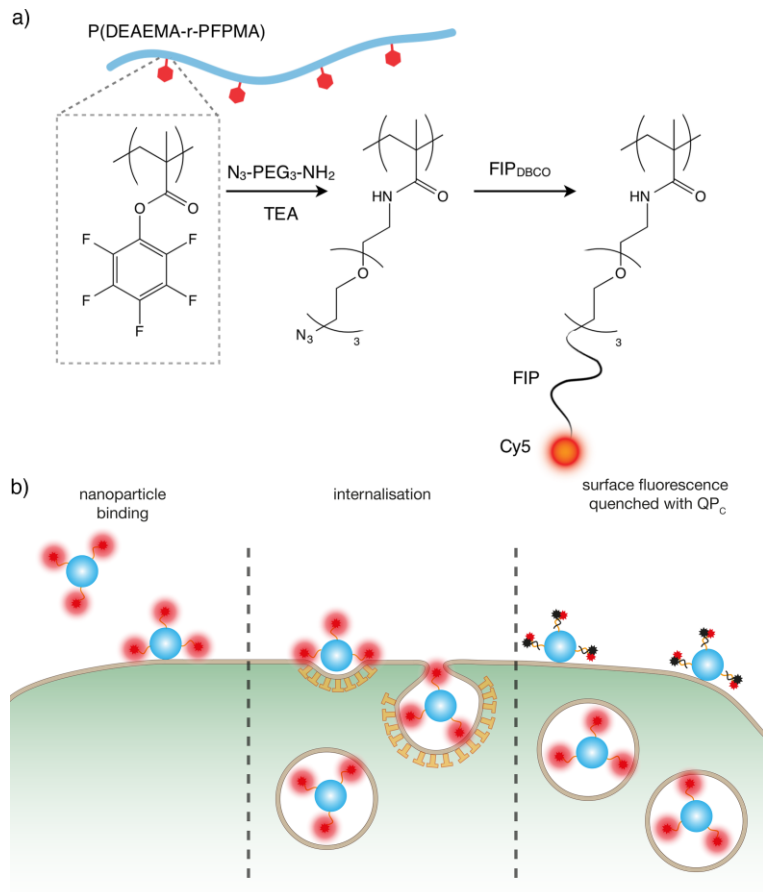












Supplementary information for:

## Quantifying Nanoparticle Internalization using a High Throughput Internalization Assay

Sarah K. Mann<sup>1,2,3</sup>, Ewa Czuba<sup>1,3</sup>, Laura I. Selby<sup>1,3</sup>, Georgina K. Such<sup>\*2</sup> and Angus P. R. Johnston<sup>\*1,3</sup>

<sup>1</sup>Drug Delivery, Disposition and Dynamics, Monash Institute of Pharmaceutical Sciences, Monash University, Parkville, Victoria 3052, Australia. E-mail: angus.johnston@monash.edu

<sup>2</sup>Department of Chemistry, The University of Melbourne, Parkville, Victoria 3010, Australia.

E-mail: gsuch@unimelb.edu.au

<sup>3</sup>ARC Centre of Excellence in Convergent Bio-Nano Science and Technology, Monash University, Parkville, Australia

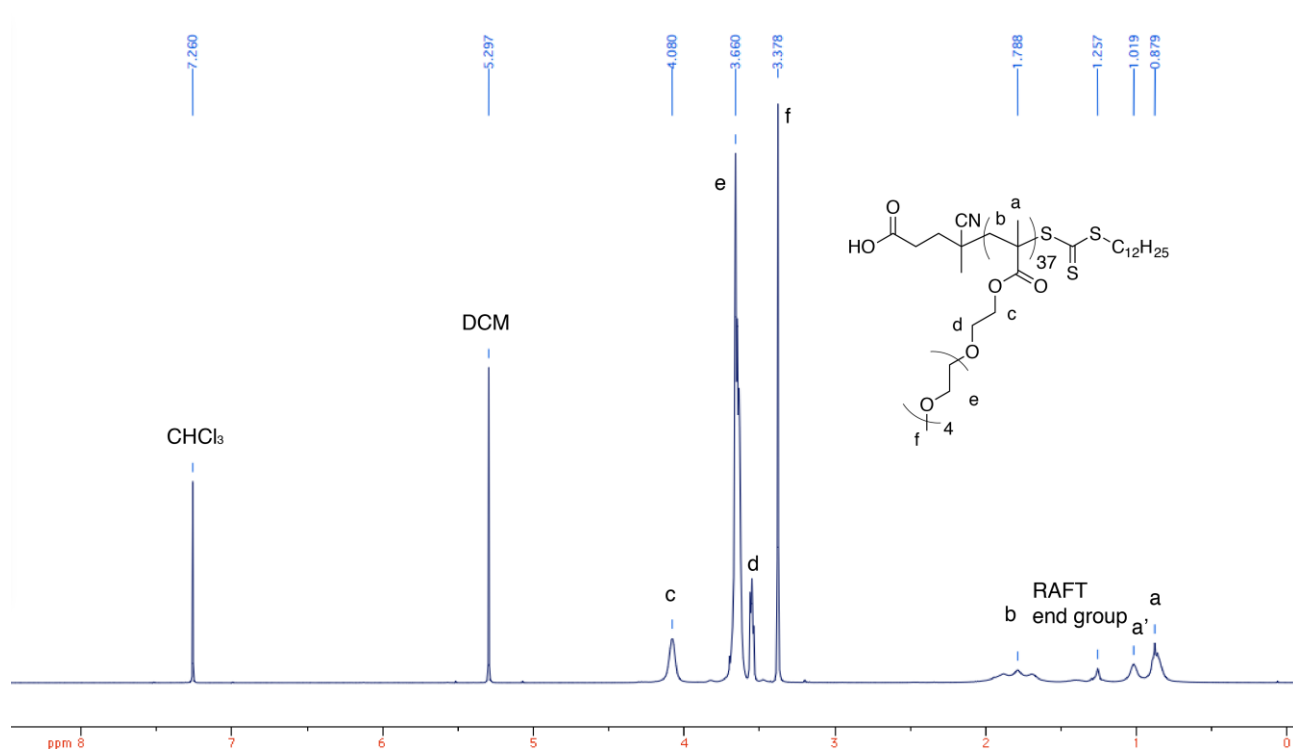


**Figure S1.** <sup>1</sup>H NMR of PEGMA<sub>37</sub> macro RAFT agent (CDCl<sub>3</sub>).

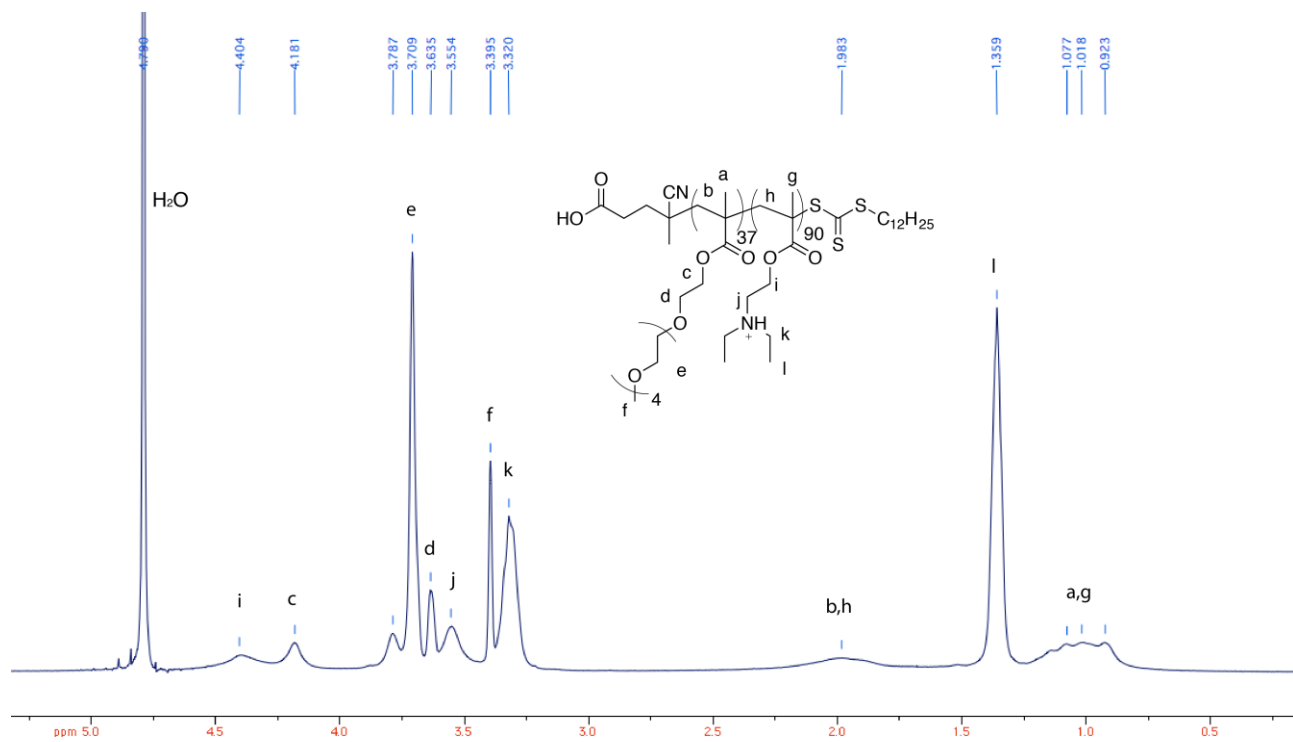


**Figure S2.** <sup>1</sup>H NMR of PEGMA<sub>37</sub>-b-PDEAEMA<sub>90</sub> (D<sub>2</sub>O).

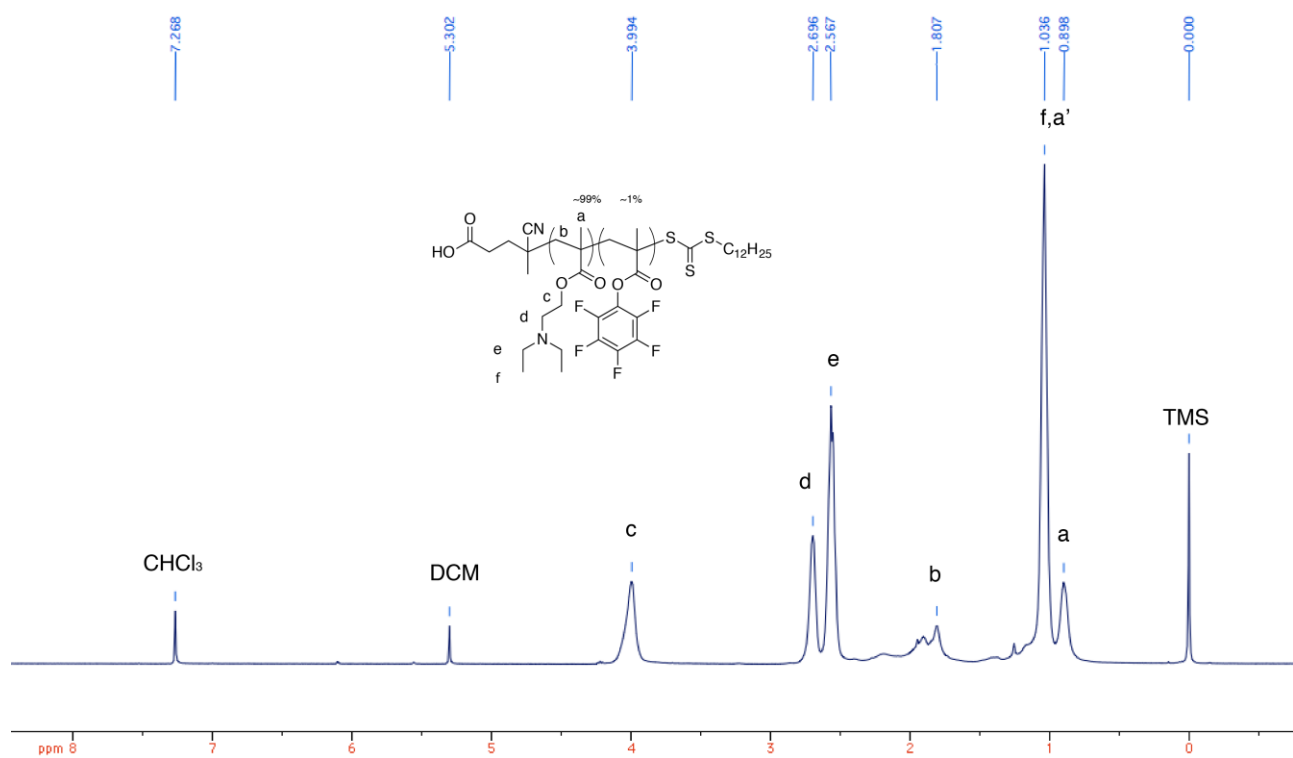


**Figure S3.**  $^1\text{H}$  NMR of P(DEAEMA-*r*-PFPMA) ( $\text{CDCl}_3$ ).

**Table S1.** Polymer characterization

Polymer	$^a\text{M}_n$ (PEG/PEGMA)	$^a\text{M}_n$ (DEAEMA)	$^b\text{PDI}$
PEGMA <sub>37</sub>	2,400	-	NA
PEGMA <sub>37</sub> - <i>b</i> -PDEAEMA <sub>90</sub>	11,100	16,700	1.64
P(DEAEMA- <i>r</i> -PFPMA)	-	49,000	NA
PDEAEMA	-	36,000	1.65

$^a$ Molecular weight ( $\text{M}_n$ ) was determined by  $^1\text{H}$  NMR;  $^b\text{PDI}$  was determined by GPC

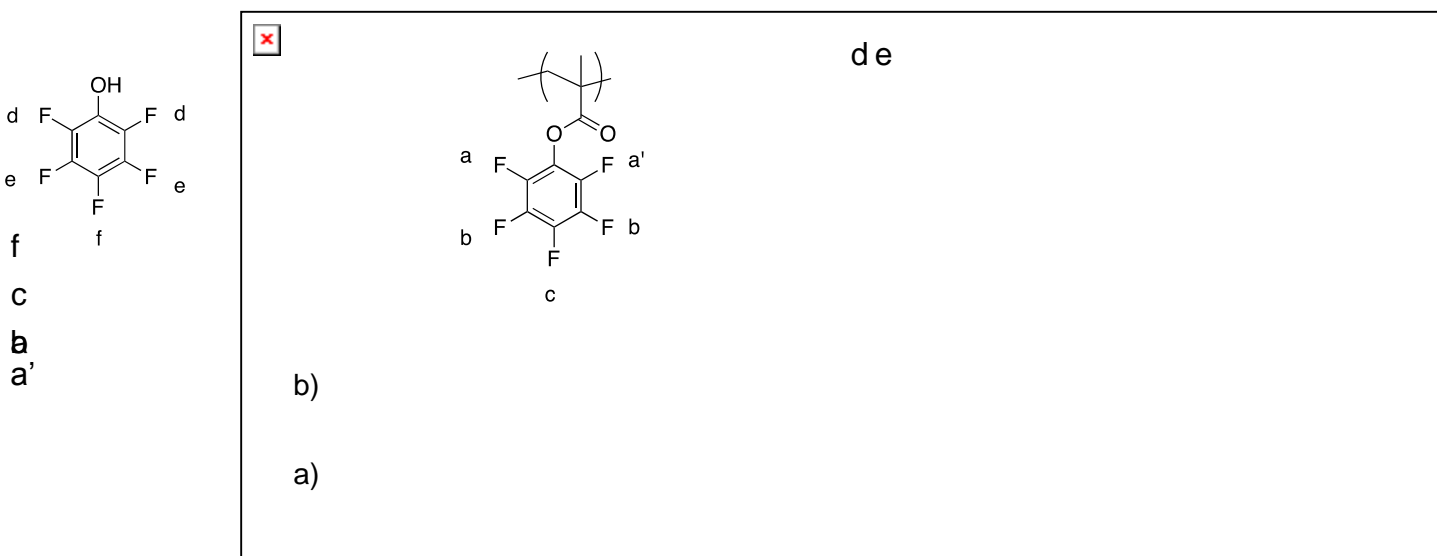


**Figure S4.**  $^{19}\text{F}$  NMR analysis of post polymerization modification of P(DEAEMA-*r*-PFPMA) with Azido-PEG3-amine. (a) P(DEAEMA-*r*-PFPMA) before modification. (b) Crude reaction mixture after 48 h. The conversion of PFP ester groups was determined to be 70% by comparing the integrals of pentafluorophenol peaks to the total integral (polymer + pentafluorophenol).

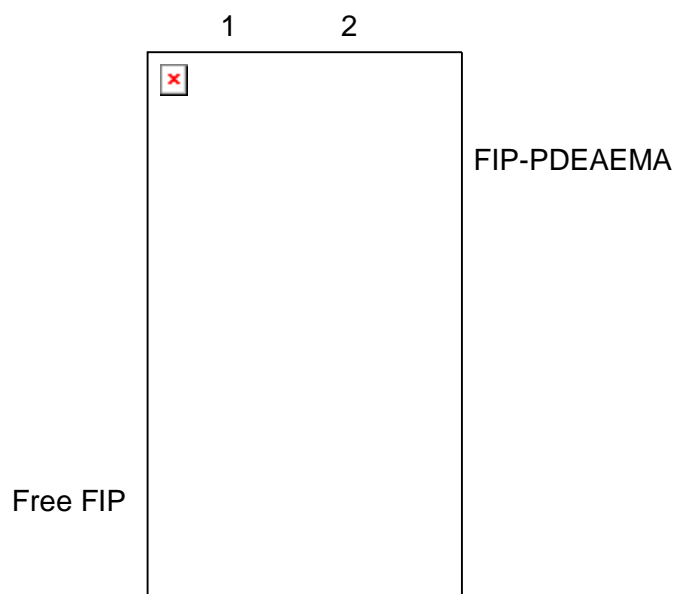
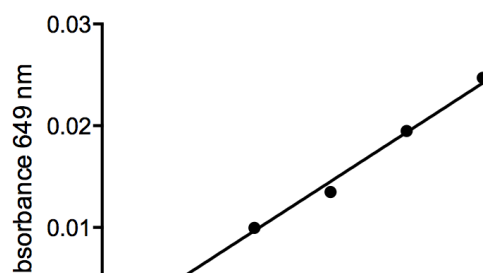


**Figure S5.** Agarose gel electrophoresis visualized by fluorescence (Lane 1: Free FIP; Lane 2: FIP-PDEAEMA).

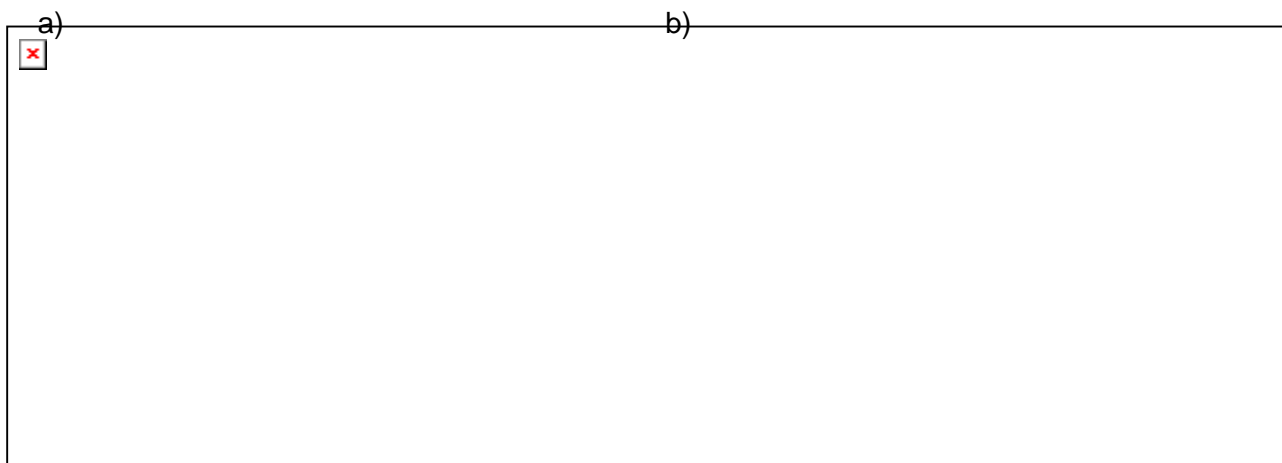
**Table S2.** Characterization of nanoparticles

Sample	Size (nm) <sup>a</sup>	PdI <sup>a</sup>	$\zeta$ <sup>b</sup> (mV)
FIP-NPs	155 ± 4	0.06	-2.8 ± 0.3
Cy5-NPs	119 ± 2	0.05	-5.4 ± 0.3
Unmodified NPs	150 ± 6	0.08	-2.7 ± 0.4

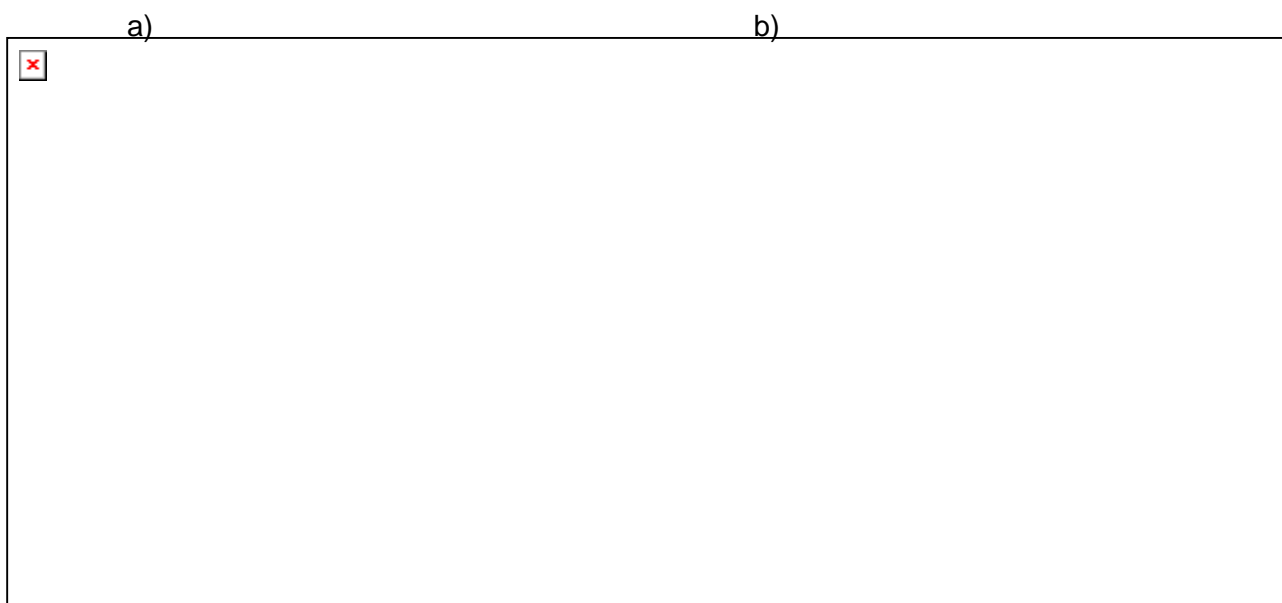
<sup>a</sup>NP size and polydispersity (PdI) were measured in PBS pH 8 at 37°C. <sup>b</sup>Zeta potential ( $\zeta$ ) was measured in 10 mM phosphate buffer pH 8 at 25°C. (n = 3, reported as mean ± standard deviation).



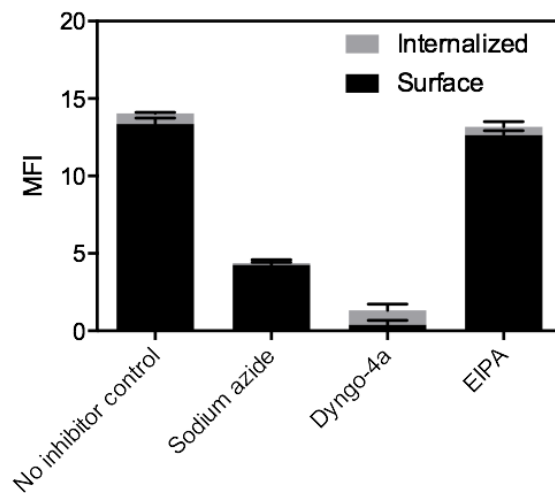
**Figure S6.** Absorbance standard curve of FIP-PDEAEMA measured at 649 nm in PBS (pH 6).



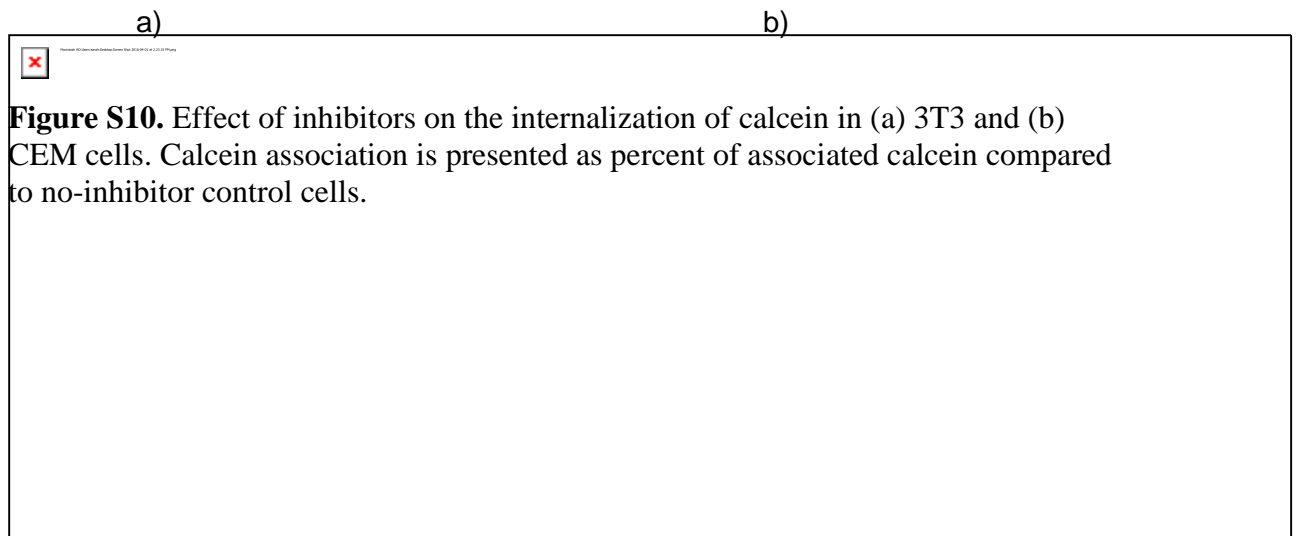
**Figure S7.** Alamar Blue cytotoxicity assay for (a) 3T3 and (b) CEM cells showing relative viability after incubation with FIP-functionalized nanoparticles for 4 hours.



**Figure S8.** Viability of (a) 3T3 and (b) CEM cells from the chemical inhibitor assay measured by PI staining.



**Figure S9.** Effect of inhibitors on the association and internalization of NPs in CEM cells.



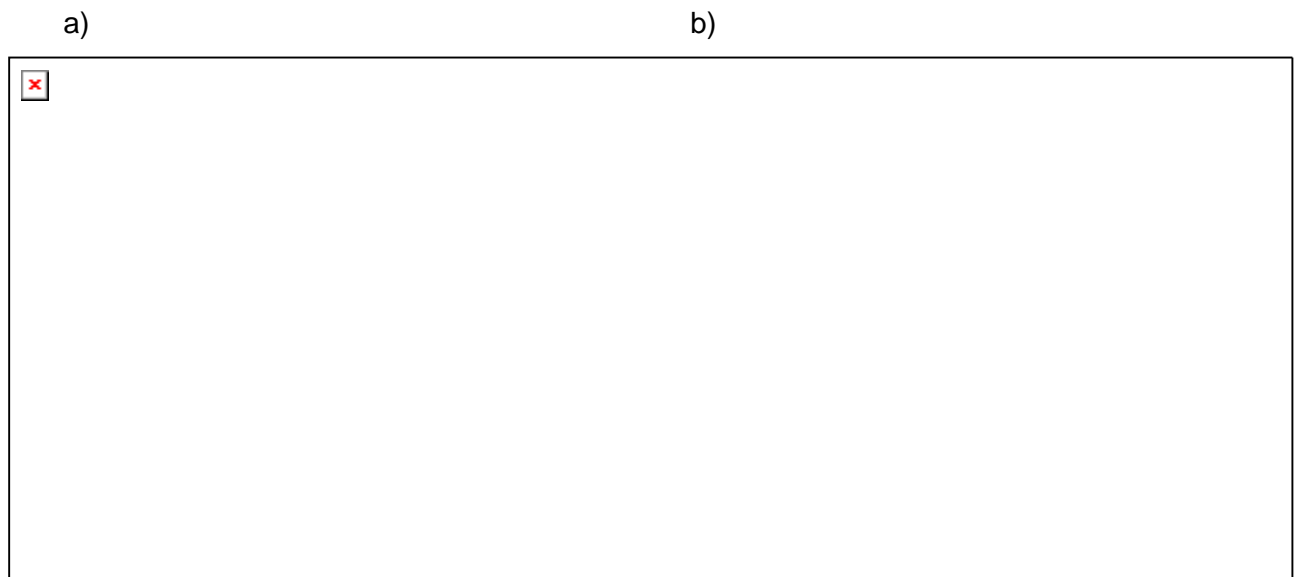


**Figure S11.** Effect of inhibitors on the internalization of Tf in 3T3 cells. (a) Analysis of surface-association and internalized Tf. (b) Tf internalization presented as percent of internalized Tf compared to no-inhibitor control cells.

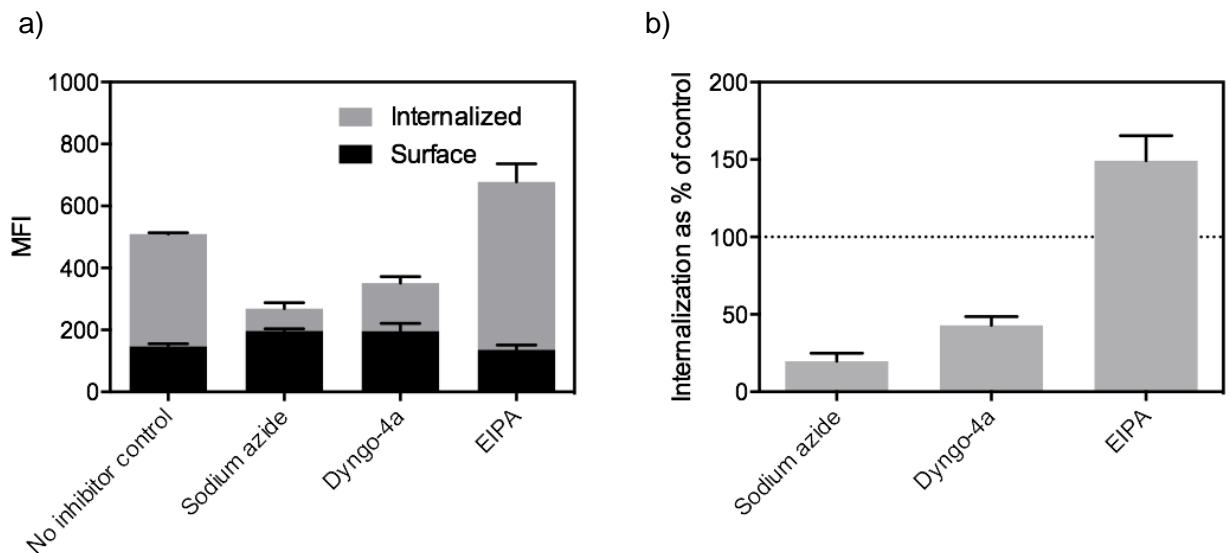


**Figure S12.** Effect of inhibitors on the internalization of Tf in CEM cells. (a) Analysis of surface-association and internalized Tf. (b) Tf internalization presented as percent of internalized Tf compared to no-inhibitor control cells.

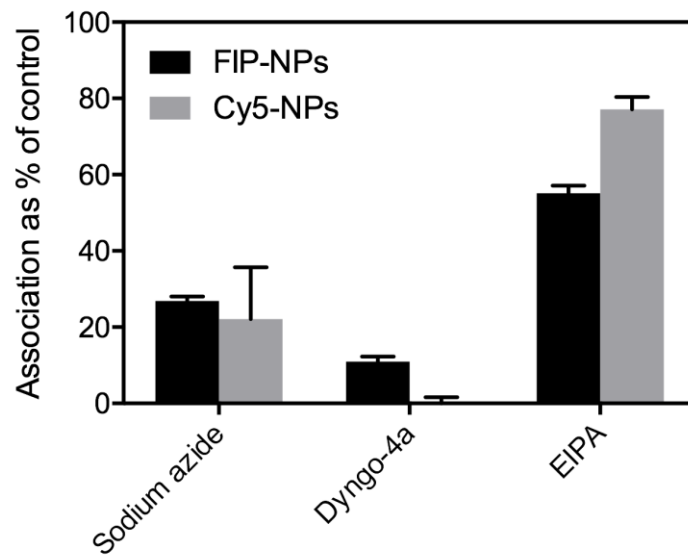


**Figure S13.** Total association of Cy5-NPs and FIP-NPs in the presence of inhibitors in 3T3 cells presented as a percent of the no-inhibitor control.